Available online at www.sciencedirect.com
SCIENCE DIRECT®
Journal of Catalysis 220 (2003) 35–43
JOURNAL OF CATALYSIS
www.elsevier.com/locate/jcat

Flame-made nanocrystalline ceria/zirconia: structural properties and dynamic oxygen exchange capacity

Wendelin J. Stark,[a,b] Marek Maciejewski,[a] Lutz Mädler,[b] Sotiris E. Pratsinis,[b] and Alfons Baiker[a,*]

[a] *Institute for Chemical and Bioengineering, ETH Hönggerberg, CH-8093 Zurich, Switzerland*
[b] *Particle Technology Laboratory, ETH Zentrum, CH-8092 Zurich, Switzerland*

Received 2 January 2003; revised 20 May 2003; accepted 20 May 2003

Abstract

Ceria/zirconia nanocrystals were prepared by flame-spray synthesis. Application of carboxylic acid-derived solvents allowed the continuous production of homogeneous mixed oxides with narrow particle-size distribution. The high preparation temperature favored the formation of a highly crystalline solid solution of the constituents. Structural and textural properties of the ceria-zirconia nanoparticles were characterized by high-resolution electron microscopy, nitrogen adsorption, and X-ray diffraction. The redox properties of the nanoparticles were investigated by temperature-programmed reduction and by dynamic oxygen exchange capacity (OEC) measurements using H_2, CO, and propene as reductants. For CO and H_2 a similar reduction was found, whereas propene afforded a considerably higher degree of reduction. While the flame-made powders had very stable specific surface area (up to 80 m^2/g) even after severe calcination (2 h at 900 °C in air) their OEC was lower than in corresponding ceria-zirconia prepared by coprecipitation. This difference is traced to the high crystallinity and low defect concentration of the flame-made material.

Keywords: Ceria/zirconia mixed oxide; Flame-spray synthesis; Nanoparticles; Structural stability; Oxygen exchange capacity; Pulse thermal analysis

1. Introduction

The current new generation of three-way catalysts (TWC) uses ceria/zirconia as key components for its high dynamic oxygen exchange capacity [1]. In the treatment of noxious gases from car exhaust, the ceria switches between its two major oxidation states Ce(III) and Ce(IV) [2]. The temperature in a typical automotive exhaust rapidly changes and very high temperature causes severe thermal stress. Therefore, stability is a major issue in TWC research as reflected in a wealth of scientific papers. It is well established that formation of ceria-zirconia solid solution greatly enhances reducibility of the ceria [2]. Different production methods, however, lead to different molecular mixing of ceria and zirconia and varying contents of defects and cracks in the material. Maximum stability is found for intensively mixed powders forming a stable solid solution of the constituents.

Coprecipitation of ceria/zirconia can lead to mixed oxide powders with extremely high specific surface area [3,4]. Unfortunately, the temperature stability of as-prepared oxides is characterized by a severe loss of surface area at elevated temperature. Preparation at high temperature may produce an oxide with increased stability. This has prompted several authors to prepare ceria and ceria containing oxides by flame methods which led to a series of patents [5–10]. These methods either use expensive precursors, such as alkoxides [8, 9], demanding atomization devices [7,11] and tend to produce inhomogeneous powders containing large lumps [10]. Aruna et al. investigated the ceria/zirconia synthesis by combusting mixtures of redox compounds (urea) and oxidizing metal precursors (nitrates) [12]. This high temperature preparation yielded a high surface area product with excellent phase mixing. It is a batch process, however, and explosion hazard causes great difficulties. Laine et al. prepared ceria/zirconia by flame spray synthesis but the specific surface area of the product powder stayed low, typically at 10 to 15 m^2/g [13,14]. Sutorik et al. [15] very recently produced ceria/zirconia mixed oxides by flame spray synthesis

* Corresponding author.
E-mail address: baiker@tech.chem.ethz.ch (A. Baiker).

0021-9517/$ – see front matter
doi:10.1016/S0021-9517(03)00235-5

showing formation of solid solutions, but obtained rather low specific surface area while no tests on the oxygen exchange capacity were undertaken. It was shown recently that complex mixed oxides with high specific surface areas could be prepared at even higher temperatures by using continuous flame and flame-spray pyrolysis [16].

Here, we report the use of continuous flame-spray pyrolysis for production of high specific surface area ceria/zirconia from low-cost precursors [17,18] and compared them to samples prepared by coprecipitation [19]. Since volatile organic components (VOC) are a major component in automotive exhaust gas, the role of propene is investigated as a reductant in OEC measurements beside CO and hydrogen.

2. Experimental

2.1. Preparation of mixed oxides

Ceria/zirconia mixed oxide powders were produced by flame-spray pyrolysis in a laboratory scale setup [17]. Cerium (III) acetate hydrate (Aldrich, > 99.7%) and zirconium tetraacetylacetonate (Aldrich, 99%) were mixed according to the product composition and dissolved in a lauric/acetic acid mixture (1/1 by weight), heated to full dissolution resulting in a total metal concentration of 0.15 M. In a preliminary study [18], the lauric/acetic acid mixture proofed to be the most suitable carrier liquid for the production of high surface area ceria/zirconia. Solutions were delivered into the flame at 5 ml/min by a syringe pump (Inotec R 232) and atomized by 5 L/min oxygen (Pan Gas, 99.8%) dispersion gas. The apparatus [17] consisted of a central spray delivery (two-phase nozzle), a premixed, circular support flame (diameter 6 mm, slit width 10 μm), and a circular sheet gas delivery (ring of sinter metal, inner diameter 11 mm, outer diameter 18 mm, 5 L/min oxygen). A mixture of methane (1.5 L/min, Pan Gas, 99%) and oxygen (2 L/min) was fed to the inner slit and formed the premixed flame. All gas flow rates were controlled by calibrated mass flow controllers (Bronkhorst EL-Flow F201). Powders were denoted as $Ce_xZr_{1-x}O_2$, where x ($0 < x < 1$) is the amount of ceria in the samples. Depending on composition, a nominal production rate of 3.3 to 4.6 g/h was achieved.

Reference samples were prepared by coprecipitation according to Leitenburg et al. [19]: In brief, corresponding solutions of cerium nitrate (Fluka, > 99.5%) and zirconium oxynitrate (Fluka, > 99%) in distilled water at a total concentration of 0.2 M were dropped into concentrated aqueous solution of ammonia (24 mass%) under stirring. The solutions were filtered after 2 h and washed with distilled water 6 times. The yellowish to white slurry was dried at 200 °C for 2 h.

2.2. Characterization

2.2.1. Specific surface area and isotherms

The specific surface areas of the collected powders were analyzed by nitrogen adsorption at 77 K using the BET method (Micrometrics Gemini 2360). The results were cross-checked by recording a full adsorption isotherm (Micrometrics ASAP 2010 Multigas system).

2.2.2. High-resolution electron microscopy

The HRTEM investigations were performed on a CM30ST microscope (Philips, LaB6 cathode, 300 kV, point resolution 2 Å). Particles were deposited onto a carbon foil supported on a copper grid.

2.2.3. X-ray diffraction

XRD diagrams were measured on a Bruker D 8 Advance diffractometer (Cu-K_α radiation) from 20 to 75° at a step size of 0.02° and a scan speed of 0.24°/min. Crystallite characteristics and average crystal size were obtained from the XRD diagram using the Topas 2.0 software (Bruker AXS, 2000) by the fundamental parameter approach (Rietveld method).

2.2.4. Thermal analysis (TA)

Thermoanalytical experiments were carried out both isothermally and nonisothermally (heating rates 3, 5, or 10 K/min) on a Netzsch STA 409 thermoanalyzer equipped with a gas injector (PulseTA box, Netzsch) which allows for the injection of a defined sample gas volume into the carrier gas stream [21]. If not stated otherwise, the amount of injected gases (hydrogen, oxygen, propene, carbon monoxide) was 1.0 ml. The total reduction of the samples was carried out in the atmosphere of 20 vol% H_2, balance Ar with a rate of 5 K/min in the range 300–1075 °C. Gases evolved during reaction and/or injected into the system were monitored online with a Balzers QMG 420 quadrupole mass spectrometer connected to the thermoanalyzer by a heated (ca. 200 °C) capillary.

3. Results

3.1. Structural properties

Spraying corresponding mixtures of cerium and zirconium containing precursor solutions into a methane/oxygen flame continuously produced ceria/zirconia nanoparticles. Fig. 1 (left side) depicts transmission electron micrographs of as-prepared ceria/zirconia $Ce_{0.5}Zr_{0.5}O_2$. The product consists of well-crystalline, sharp-edged nanoparticles of 4–10 nm size [18]. Fig. 1 (right side) further shows the same powder after sintering at 900 °C for 2 h in air. Regularly shaped particles of high crystallinity are obtained as the high-resolution images (bottom) reveal. They are similar to

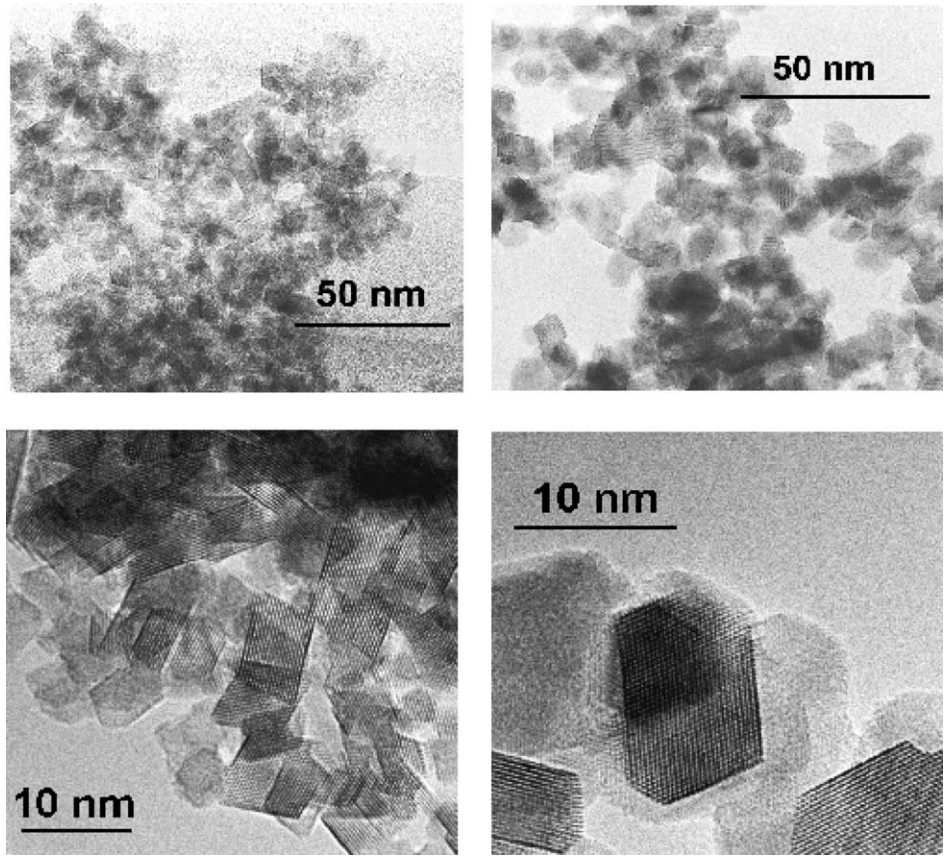

Fig. 1. High-resolution electron micrographs of as-prepared $Ce_{0.5}Zr_{0.5}O_2$ (left), and corresponding samples after sintering at 900 °C, 2 h in air (right). The crystallites at high magnification are shown on the bottom: Flame-made ceria/zirconia forms highly crystalline nanoparticles of narrow particle-size distribution. Sintering affords well-defined, regular crystallites of about 10 nm diameter. Surfaces are well-structured and flat; no defects or twinned crystals appear.

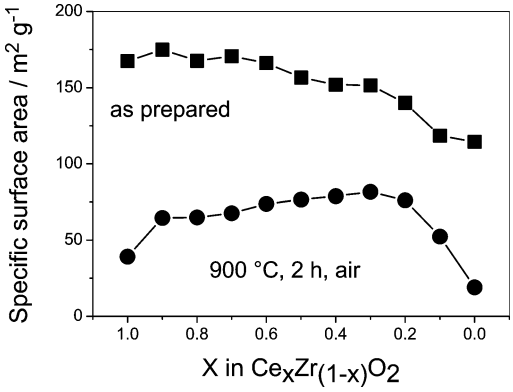

Fig. 2. Specific surface area of mixed oxide samples as prepared and after calcination ranging from pure ceria (left) to pure zirconia (right). While as-prepared particles are of similar size since the density of zirconia is higher than that of ceria, a considerable loss of specific surface area is found for the pure oxides upon sintering. Mixed oxides are rather stable and conserve up to 80 m^2/g surface area after 2 h at 900 °C in air.

earlier studies of flame-spray-made pure ceria nanoparticles [17].

Fig. 2 shows the specific surface area of as-prepared $Ce_xZr_{1-x}O_2$ (squares) and calcined powders (circles, 900 °C, 2 h in air) as a function of the Ce content x. Powders with specific surface area up to 170 m^2/g were obtained that decreased with higher zirconia content. The corresponding particle sizes were similar since the density of zirconia (5.9 g/cm^3) is lower than that of ceria (7.1 g/cm^3). After sintering in air at 900 °C for 2 h the pure constituents lost much specific surface area, whereas mixed oxides were more stable and conserved up to 82 m^2/g for $x = 0.3$.

Fig. 3A shows the XRD patterns of ceria/zirconia $Ce_xZr_{1-x}O_2$ ranging from pure ceria ($x = 1$, bottom) to pure zirconia ($x = 0$). The broad signals from the cubic ceria phase slowly shift to higher theta values. Considerable transition occurs leading to widening of the peaks. At high zirconia content ($x = 0.2$ and 0.1) the mixed oxides show some indication of phase instability and weak reflections of pure zirconia appear on top of the reflections of the solid solution phase.

Fig. 3B gives the XRD results for calcined ceria/zirconia (900 °C, 2 h, air). The reflections generally narrow due to larger crystallite size. Samples of high ceria content ($x > 0.7$) exhibit a ceria-like XRD pattern with shifted position of reflections. At intermediate composition ($0.4 < x < 0.8$) broad reflections appear and a transition from ceria-like to zirconia-like patterns can be observed. At high zirconia content ($x = 0.2$ and 0.1) the diffractogram resembles the pat-

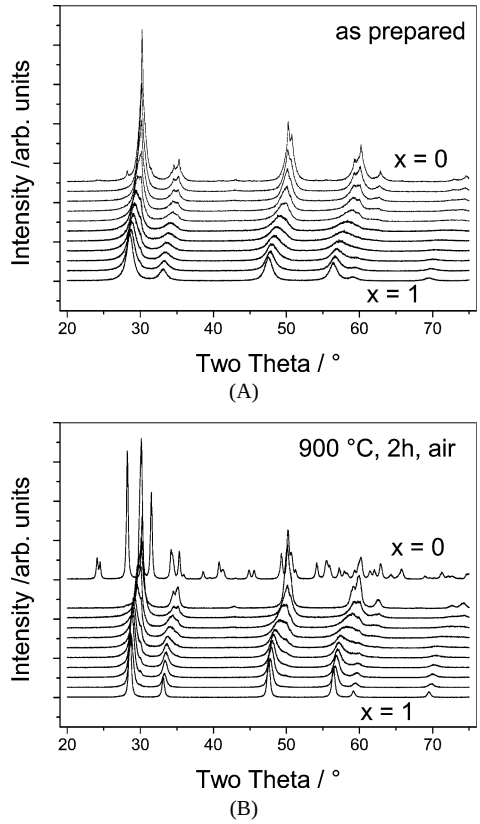

Fig. 3. X-ray diffraction pattern of as-prepared ceria/zirconia ranging from pure ceria ($x = 1$) to pure zirconia ($x = 0$). (A) As prepared, a continuous shift in peak reflections corroborates the mixing of ceria and zirconia. (B) After calcination in air at 900 °C. Powders containing up to 80% zirconia are stable against phase transformation. At 90% zirconia a small peak split indicates the onset of a new phase. Pure zirconia undergoes a transformation to the tetragonal and monoclinic phase.

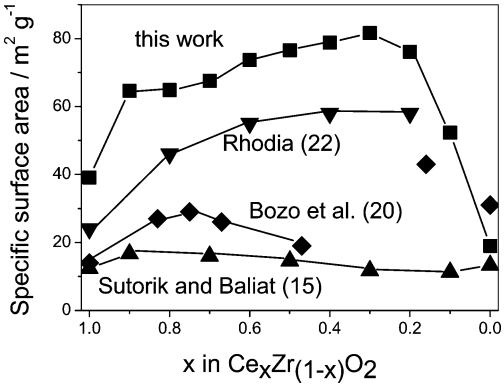

Fig. 4. Specific surface area of different ceria/zirconia prepared by precipitation of the corresponding nitrates (diamonds [20]), commercial products from Rhodia (down triangles [22]), and flame-made ceria/zirconia from Sutorik and Baliat (up triangles [16]), and this work (squares).

tern of tetragonal zirconia. Pure zirconia ($x = 0$, top line) exhibits the typical pattern of monoclinic zirconia while retaining some tetragonal phase and obviously consists of a mixture of the two modifications.

Fig. 4 further compares the specific surface area of flame-spray-made ceria, ceria/zirconia, and precipitated mixed oxides. The flame-made oxides from this study exhibit high specific surface area in a wide range of compositions. For comparison a commercial catalyst from Rhodia is shown after calcination for 6 h at 900 °C. Leitenburg et al. [19] and Bozo et al. [20] precipitated ceria/zirconia from the corresponding nitrates and achieved up to 26 m^2/g after calcination at 900 °C for 2 h in air. Note that flame-spray-made powders of previous studies report specific surface area of about 10 m^2/g [14,16] even without calcination.

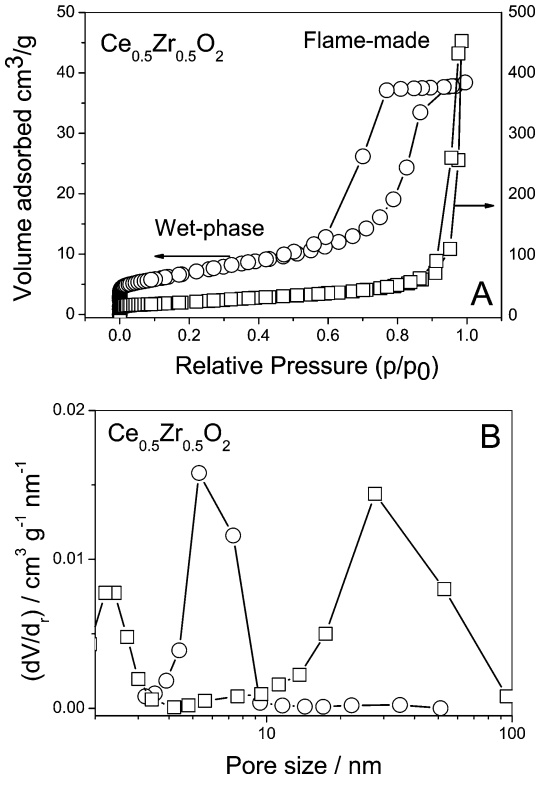

Fig. 5. (A) Adsorption isotherms of flame-made (squares, Type IV according to IUPAC) and precipitated $Ce_{0.5}Zr_{0.5}O_2$ (Type I). (B) Corresponding pore-size distributions as calculated from the isotherms. The precipitated material contains a large number of mesopores. The flame-made material shows almost no micropores which is consistent with the observation of dense, rather regularly shaped particles (Fig. 1).

Fig. 5A compares the nitrogen adsorption/desorption isotherms of $Ce_{0.5}Zr_{0.5}O_2$ prepared by precipitation (circles) and by flame-spray synthesis (squares). According to IUPAC, the precipitated sample is characterized by a Type I isotherm with prominent hysteresis. The flame-made sample exhibits a Type IV isotherm with a weak hysteresis. Fig. 5B depicts the corresponding differential pore size distribution of precipitated and flame-made ceria/zirconia. While the precipitated sample contains mainly pores of 4–10 nm in diameter and few pores at higher diameters, the flame-made sample shows few small pores probably originating from necks between particles and the largest contribution from interparticle pores 20–100 nm in diameter.

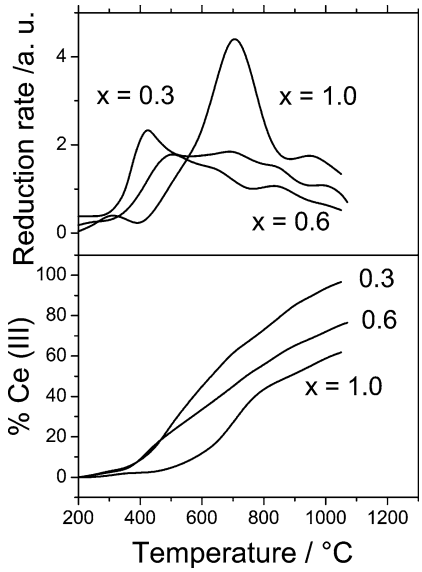

Fig. 6. Reduction behavior of flame-made ceria/zirconia. On top, the reduction rate of 50-mg samples of increasing temperature is shown. The degree of reduction calculated for the ceria in the sample is indicated at the bottom. Pure ceria is characterized by a prominent peak at ca. 700 °C. Adding zirconia results in a much lower reduction temperature.

3.2. Redox properties

Fig. 6 depicts reduction rate (top) and reduction profiles (bottom) for pure ceria (CeO_2), 40% ceria/zirconia ($Ce_{0.6}Zr_{0.4}O_2$), and 70% ceria/zirconia ($Ce_{0.3}Zr_{0.7}O_2$) measured under 20 vol% hydrogen in argon on a thermobalance. The reduction rate is obtained by differentiating the TG curve. Pure ceria shows a single reduction peak at 700 °C. The degree of ceria reduction calculated from the mass loss (TG) is presented as a function of temperature. Zirconia is not reduced in the range 200–1100 °C. The increase of zirconia content promotes the reduction of ceria, the sample $Ce_{0.3}Zr_{0.7}O_2$ was almost fully reduced to Ce(III) above 1000 °C.

Fig. 7 illustrates the principle of dynamic oxygen storage capacity measurements performed on the TG-MS system using the pulse TA technique [21]. Reduction is very fast for all reducing agents (hydrogen, CO, and propene) and steady state is attained very fast. After oxidation, the sample mass reaches exactly the same level as prior to the experiment corroborating full reversibility of the redox process. The appearance of a strong hydrogen signal ($m/z = 2$) in the MS trace indicates that excess hydrogen was provided in the pulse. Incomplete conversion could be excluded by applying a second hydrogen pulse that did not cause further reduction. While hydrogen and CO result in a comparable degree of reduction, propene removes much more oxygen and two O_2 pulses are needed for reoxidation.

Fig. 8 gives the dynamic oxygen exchange capacity (OEC) of ceria/zirconia for 11 samples ranging from pure ceria (left, $x = 1$) to pure zirconia (right, $x = 0$) for flame-made oxides (filled symbols) and 5 precipitated materials

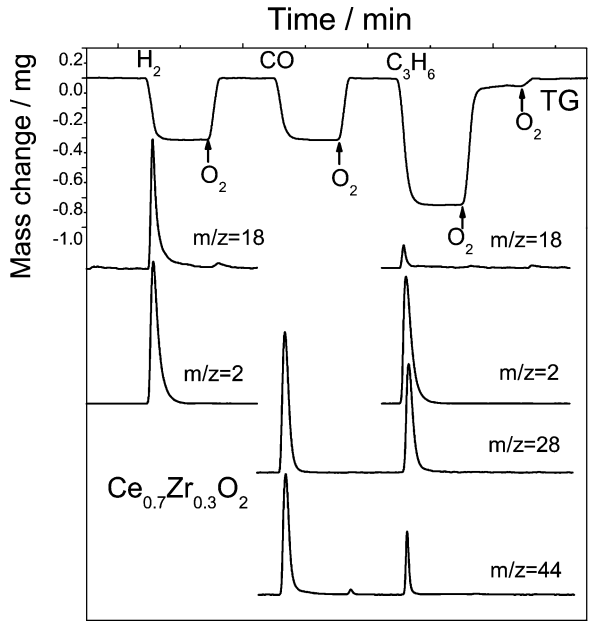

Fig. 7. Schematic presentation of measuring principle for determining the oxygen exchange capacity by pulse thermal analysis. Samples (50 mg) were reduced at 700 °C by pulses of reductant (H_2, CO, and propene) and reoxidized by pulses of O_2. Gases injected and evolved during redox processes were monitored by mass spectrometry.

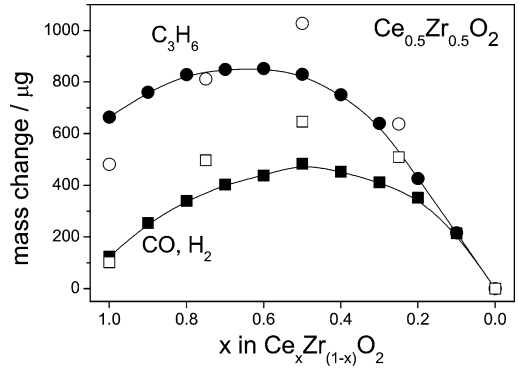

Fig. 8. Mass changes of ceria/zirconia samples (50.0 mg) resulting from pulses of the reducing agent (H_2, CO, 2 ml, propene, 1 ml) at 700 °C. After reduction the samples were fully reoxidized by 1 ml oxygen pulses.

(open symbols). Using H_2 or CO as reductant, the precipitated materials showed superior OEC compared to the flame-made ones. This tendency was less clear when using propene. At higher zirconia loading ($x < 0.2$), the differences between the results obtained with the different reduction agents disappeared, mainly due to high conversion in both cases. The maximum reducibility was found for the samples containing around 50% Ce (when reduced by CO or H_2) and about 60–75% Ce (reduction by propene).

Fig. 9 depicts high-resolution electron micrographs of precipitated $Ce_{0.5}Zr_{0.5}O_2$. The morphology may be characterized as a heavily aggregated, rather dense conglomerate of small crystallites (left). Sintering the precipitated ceria/zirconia increased its crystal size and further compacted the structure. Compared to the flame-made nanocrystals, the

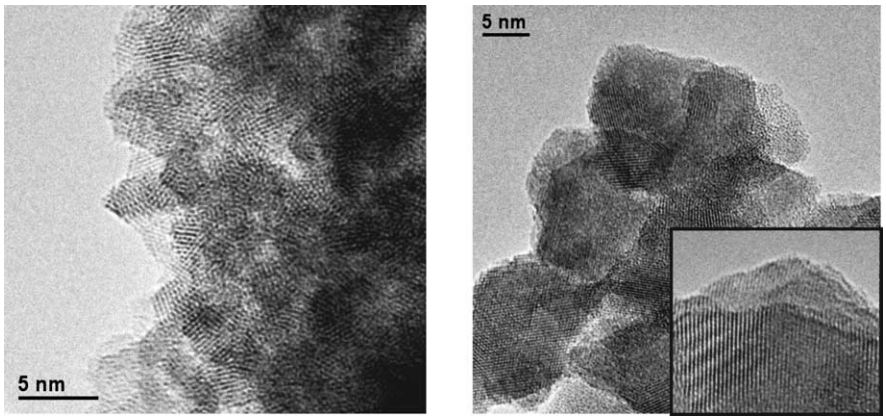

Fig. 9. High-resolution electron microscopy images of precipitated $Ce_{0.5}Zr_{0.5}O_2$ as prepared and after sintering (900 °C, 2 h in air). The fresh material consists of ill-defined, partially amorphous ceria/zirconia. Sintering results in large, heavily agglomerated and twinned crystals with a rough surface (see inset). A clear contrast is seen to the flame-made materials where a smooth surface and well-defined crystallites are observed (Fig. 1).

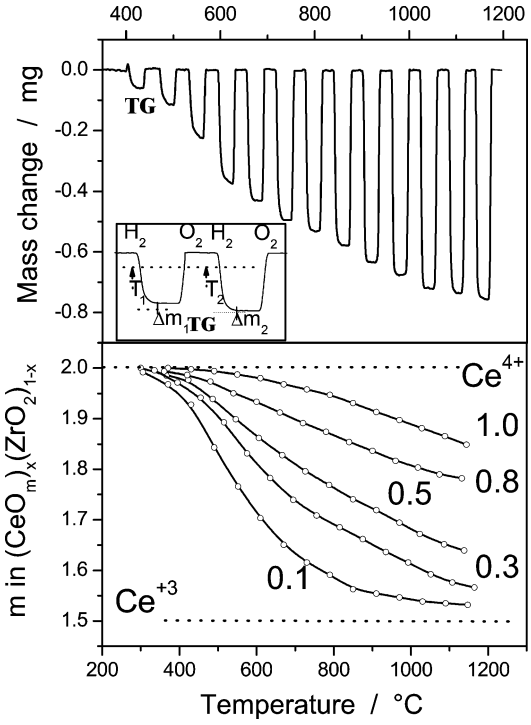

Fig. 10. Mass change of the 50-mg sample $Ce_{0.6}Zr_{0.4}O_2$ due to 4-ml pulses of hydrogen followed by 2-ml pulses of oxygen at different temperatures. The insert explains the construction of the dependence $\Delta m - T$ used for the calculation. Due to full reoxidation by the oxygen pulses, the composition of the sample is always the same prior to the hydrogen pulses.

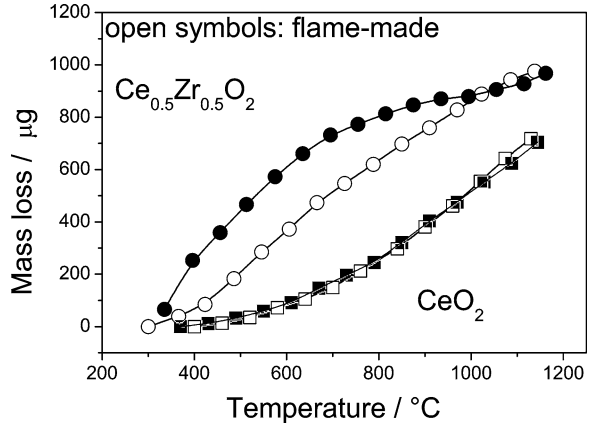

Fig. 11. Comparison of the dynamic oxygen exchange capacity of flame-made and precipitated CeO_2 and $Ce_{0.5}Zr_{0.5}O_2$ at increasing temperatures. At higher temperatures, the precipitated and flame-made materials become similar since defects are annealed in the precipitated sample due to the heat impact. In unstabilized ceria, the pretreatment step has healed out the defects rendering the precipitated similar to the flame-made ceria.

surface of the precipitated material is rather rough and irregular.

Fig. 10 shows the TG trace for several consecutive reduction-oxidation pulses for $Ce_{0.6}Zr_{0.4}O_2$ when increasing the temperature (top) from 300 to 1150 °C. The resulting degree of reduction as a function of temperature for samples ranging from pure ceria to 10% ceria/zirconia is shown in the lower part of the figure. Ceria is more reduced in zirconia-rich samples at all temperatures. As in the case of the results presented in Fig. 8, the reduction is favored by the addition of Zr.

Fig. 11 compares the dynamic oxygen exchange capacity at increasing temperature of flame-made and precipitated CeO_2 and $Ce_{0.5}Zr_{0.5}O_2$. Samples were sintered at 700 °C, 16 h in air prior to the measurements. The conventionally prepared $Ce_{0.5}Zr_{0.5}O_2$ shows a higher degree of dynamic reduction/oxidation than the flame-made samples. At higher temperature, however, the behavior of both materials is similar. In contrast, corresponding ceria samples show very similar behavior over the whole range of temperature.

4. Discussion

4.1. Flame-spray synthesis

Fig. 1 shows homogeneous nanostructured ceria/zirconia. No large lumps of ceria could be detected, corroborating

good dispersion of the metal precursor and subsequent precipitation in the flame. For pure ceria, high combustion heat of the carrier liquid is crucial for obtaining a homogeneous material [17]. A droplet entering the flame may continuously release precursor solution or an enrichment of the metal may take place if the carrier liquid (fuel) leaves the droplet first. In the latter case, a nonuniform metal concentration in the flame with locally high amounts of metal oxide may favor the formation of larger particles and broad particle-size distribution. Furthermore, if two or more metal precursors are present in the droplet, element segregation from different evaporation and decomposition rates may result in inhomogeneous products. Here, it was shown that by using an acetic/lauric acid carrier liquid instead of isooctane/acetic acid/2-butanol [17] elemental segregation and resulting phase instability could be avoided [18]. The formation of a single-phased mixed oxide with particles of few nanometers in size corroborates the excellent degree of mixing of ceria and zirconia in the flame. The continuous shift of pertinent reflections in XRD patterns (Fig. 3) confirms that this holds true for compositions up to 80% zirconia.

4.2. Structural properties

A comparison of precipitated [20], surfactant-assisted precipitated [3,4], commercial [22], and flame-made ceria/zirconia from Sutorik and Baliat [15] proves the excellent sintering stability of the flame-made nanoparticles. Thermal stability is associated with a high degree of mixing of the constituents forming the solid solution, an open morphology, and annealed crystallites with few defects [18]. The phase diagram of ceria/zirconia indicates a mixed solid solution as the stable form of intermediate ceria/zirconia mixtures for temperatures up to ca. 1000 °C [23,24]. Calcination of flame-made powders at 900 °C (Fig. 3B) did not result in significant phase separation up to 80% zirconia and therefore corroborated a good ceria distribution. The phase stability of ceria/zirconia is not straightforward and depends on the preparation method. In the case of precipitated ceria/zirconia, Bozo et al. [20] found considerable instability in the solid solution for powders calcined at 900 °C. The high degree of crystallinity of the flame-made mixed oxides is evident from Fig. 1 where lattice fringes are discernible in the high-resolution TEM images. The isotherms in Fig. 5A reflect this morphology which results in a Type IV isotherm. The low pore content observed stems from interparticle necks. The resulting pore-size distribution in Fig. 5B depicts a significant contribution from mesopores 20–100 nm in diameter. From the HRTEM (Fig. 1) these can be associated with the voids between the crystallites. The rather regular shape of the calcined powders results in a material where well-structured crystalline surfaces (Fig. 1) do not facilitate sintering. The well-defined crystallites are of similar size, few smaller crystallites are prone to sintering and lead to a drop in specific surface area. Laine et al. [6,13] used flame-spray pyrolysis to make a series of oxide powders and presented a low-cost route to ceria/zirconia. They used an ultrasonic mister to aerolize ethanol-based precursor solutions. Metal precursors were kept in solution as separately produced derivatives of tris-ethanolamin. The process resulted in rather large, unagglomerated ceria/zirconia with a specific surface area of 10 m^2/g but at larger production rates than reported here. Besides providing a one-step preparation, the carboxylic acid-derived solvent (acetic/lauric acid) used in this study has a higher combustion heat, allowing higher temperature and faster gas flow in the flame-spray reactor. Consequently, shorter residence time limits particle growth, thus favoring smaller particles. With carboxylic acid's potential for violent droplet explosions, it may favor the homogeneous distribution of the precursors in the flame [18].

4.3. Reduction behavior

Even though Hickey et al. [25] recently showed that temperature-programmed reduction (TPR) provides a rough estimate of oxygen storage capacity, at best, the reduction profiles give some indication on the type and abundance of different ceria species in a sample. In Fig. 6, pure flame-made ceria showed a prominent reduction peak at around 700 °C. According to Giordano et al. [26], this ceria may be classified as low-surface area ceria (LSA), based on its reduction behavior. Their LSA ceria had a specific surface area of 3 m^2/g, whereas the flame-made ceria with a very similar reduction behavior exhibits 39 m^2/g. The high surface area ceria (HSA) reported by Giordano et al. [26] had a specific surface area of 44 m^2/g. Its reduction behavior was characterized by an additional, large reduction signal at 500 °C. Interestingly, the flame process affords a high surface area ceria with otherwise similar characteristics as classical LSA ceria.

For mixed ceria/zirconia, Fornasiero et al. [27] reduced precipitated $Ce_{0.5}Zr_{0.5}O_2$ with hydrogen and found maximum hydrogen uptake at 400 and 630 °C. Similarly, Hickey et al. [28] reported maximum reduction at 520 to 570 °C for precipitated $Ce_{0.6}Zr_{0.4}O_2$ of only 4 m^2/g surface area. Commercial Rhodia $Ce_{0.5}Zr_{0.5}O_2$ is reduced at around 500 °C [29] and the amount of Ce(III) formed at 700 °C increased from 20 (CeO_2) to 77% ($Ce_{0.5}Zr_{0.5}O_2$) [29], depending on the composition. The dependence of reduction progress of the flame-made materials increased from 27 (CeO_2) to 44% ($Ce_{0.6}Zr_{0.4}O_2$). Similarly, the LSA ceria of Giordano et al. [26] was reduced by 20% at 860 °C, whereas the flame-made pure ceria showed 47% reduction at the same temperature. Consequently, the overall reduction behavior of flame-made ceria/zirconia is similar to conventionally prepared catalysts. In the case of pure ceria, however, the high-surface flame-made oxide can be better reduced showing to some extent the role of surface area in reduction.

4.4. Dynamic oxygen exchange capacity

Dynamic oxygen storage capacity was measured using H_2, CO, and propene as reducing agents. The smooth de-

pendence of the OEC on the ceria content (Fig. 8) reflects the homogeneity and intimate mixing of the flame-made oxides as indicated by HRTEM (Fig. 1), specific surface area (Fig. 2), and XRD (Fig. 3). The highest oxygen exchange activity using H_2 or CO was found for $Ce_{0.5}Zr_{0.5}O_2$, i.e., for intermediate compositions of ceria/zirconia. This observation correlates well with Boaro et al. [30] who investigated the CO-OEC of fresh ceria/zirconia (Rhodia) with 92–108 m^2/g, aged samples with 41–68 m^2/g, and well-aged samples with low specific surface area (10–18 m^2/g). While the OEC strongly depended on the aging and specific surface area, the maximum OEC was found for high and intermediate surface area samples with 68% ceria. The low surface area samples showed a shifted maximum OEC toward 70–80% ceria. Interestingly, our flame-made oxides behaved as the freshly prepared samples of Boaro et al. [30], even after severe sintering for 16 h at 700 °C in air. While the absolute values are difficult to compare since different techniques were used, this qualitative comparison corroborates the increased stability of the flame-made samples.

Using a stronger reductant, propene, a considerably higher degree of ceria reduction was observed for all samples. At high ceria content, the effect was most pronounced since only low conversions were achieved using H_2 or CO. At low ceria content, the reduction is favored to the point that even H_2 or CO afford higher conversions. Adding a stronger reductant consequently could not further increase conversion and similar degrees of reduction were observed.

A direct comparison of flame-made and precipitated samples in Figs. 8 and 11 reveals the differences in reducibility for materials prepared by these two methods. These differences may be discussed in terms of defect content. The flame method produces oxides with very low defect concentration. This agrees with the reduction profiles where a LSA-type ceria with high specific surface area was found. To obtain the LSA-type ceria, Giordano et al. [26] applied a severe thermal treatment to HSA ceria. This sintering heals out defects. Consequently, the performance of flame-made materials resembles that of a well-sintered material.

The higher performance of the precipitated mixed oxides in Fig. 8 can now be explained with the aid of Fig. 11. Pure ceria, or, in other words, unstabilized ceria prepared by precipitation considerably sinters when treated at 700 °C for 16 h in air. This treatment removes the favorable defects found in precipitated materials and no marked difference in OEC is found in Fig. 11 from 300 to 1150 °C. Using propene (Fig. 8), the performance of the flame-made material is even higher since it could conserve more surface after sintering. This observation is further supported by the reduction profiles where a higher degree of reduction was found for flame-made ceria (Fig. 7) using propene. Adding zirconia presumably suppresses the defect healing during the pretreatment (700 °C/16 h/air) and defects are partially conserved. Despite the much higher specific surface area (100 m^2/g versus 24 m^2/g after the pretreatment for flame-made compared to precipitated $Ce_{0.5}Zr_{0.5}O_2$) the OEC of the precipitated materials is higher than that of the flame-made materials. Fig. 11 shows that this holds true up to about 1000 °C. Then, a considerable degree of sintering starts to remove defects even in the case of stabilized ceria ($Ce_{0.5}Zr_{0.5}O_2$). Above 1000 °C, the two samples become comparable and the flame-made material keeps increasing the OEC with temperature while the profile of the precipitated material becomes flatter. Since complete reduction would result in a mass loss of 1354 µg in Fig. 11, it can be concluded that the trend of the $Ce_{0.5}Zr_{0.5}O_2$ profile did not result from approaching full conversion (complete reduction of ceria to Ce(III)).

5. Conclusions

The production of ceria/zirconia nanocrystals by flame-spray pyrolysis affords mixed oxides of high specific surface area and improved thermal stability. Control of the major process parameters: combustion energy delivery, metal concentration, and carrier liquid (solvent) composition allow production of nanometer-sized ceria/zirconia crystals over a broad range of conditions. Product homogeneity and phase stability are directly related to a homogeneous delivery of both constituent precursors from the spray droplet into the flame. Stable solid solutions were obtained for all compositions of ceria/zirconia. Both in terms of reduction behavior and dynamic oxygen exchange capacity, the flame-made samples show similar properties as highly sintered ceria/zirconia. High-resolution electron microscopy uncovered, however, a striking different morphology. Whereas precipitated ceria/zirconia consists of irregular, heavily aggregated crystallites, the flame-made material is made up of regularly shaped single crystals of few nanometer in size. With respect to specific surface area, the flame-made nanocrystals are much more stable toward temperature impact than corresponding precipitated materials. This may pave the way to ceria/zirconia and similar ceramic materials with improved long-term stability for high-temperature catalytic applications.

Acknowledgments

We thank S. Veith for the pore-size analysis and Dr. F. Krumeich for the high-resolution transmission electron microscopy investigations. Financial support by ETH Gesuch Nr. 19/01-1 and the Swiss Commission for Technology and Innovation, Top Nano 21, Nr. 5978.2 is kindly acknowledged.

References

[1] J. Kaspar, P. Fornasiero, M. Graziani, Catal. Today 50 (1999) 285.
[2] A. Trovarelli, Catal. Rev.-Sci. Eng. 38 (1996) 439.
[3] D. Terribile, A. Trovarelli, J. Llorca, C. Leitenburg, G. Dolcetti, J. Catal. 178 (1998) 299.
[4] D. Terribile, A. Trovarelli, J. Llorca, C. Leitenburg, G. Dolcetti, Catal. Today 43 (1998) 79.
[5] E.R. Novinshi, Eur. patent 0,086,330, 1983.

[6] R.M. Laine, C.R. Bickmore, D.R. Treadwell, F. Waldner, US patent 5958361, 1995.
[7] P.R. Strutt, B.H. Kear, R.F. Boland, WO patent 97/18341, 1995.
[8] R.M. Laine, C.R. Bickmore, K.F. Waldner, US patent 5614596, 1995.
[9] A. Gutsch, T. Henning, S. Katusic, M. Krämer, G. Michael, G.J. Varga, Eur. patent 1142830 A1, 2000.
[10] C.-H. Hung, J.D. Smith, G.P. Fotou, K.C. Koehlert, WO patent 01/36332 A1, 2000.
[11] T. Yoshioka, K. Dosaka, T. Sato, A. Okuwaki, S. Tanno, T. Miura, J. Mater. Sci. Lett. 11 (1992) 51.
[12] S.T. Aruna, K.C. Patil, NanoStruct. Mater. 10 (1998) 955.
[13] R.M. Laine, T. Hinklin, G. Williams, S.C. Rand, J. Metastable Nanocryst. Mat. 8 (2000) 500.
[14] R.M. Laine, R. Baranwal, T. Hinklin, D. Treadwell, A. Sutorik, C. Bickmore, K. Waldner, S.S. Neo, Key. Eng. Mat. 159 (1999) 17.
[15] A.C. Sutorik, M.S. Baliat, Mater. Sci. Forum 386–388 (2002) 371.
[16] W.J. Stark, S.E. Pratsinis, Powder Technol. 126 (2002) 103.
[17] L. Mädler, W.J. Stark, S.E. Pratsinis, J. Mater. Res. 17 (2002) 1356.
[18] W.J. Stark, L. Mädler, M. Maciejewski, S.E. Pratsinis, A. Baiker, Chem. Commun. 588 (2003).
[19] C. Leitenburg, A. Trovarelli, J. Llorca, F. Cavani, C. Bini, Appl. Catal. A 139 (1996) 161.
[20] C. Bozo, F. Gaillard, N. Guilhaume, Appl. Catal. A 220 (2001) 69.
[21] M. Maciejewski, C.A. Müller, R. Tschan, W.D. Emmerich, A. Baiker, Thermochim. Acta 295 (1997) 167.
[22] http://www.rhodia-ec.com/site-ec-us/catalysis/page-automotive.htm, 2002.
[23] E. Tani, M. Yoshimura, S. Somiya, J. Am. Ceram. Soc. 66 (1983) 506.
[24] L. Li, O. Van Der Biest, P.L. Wang, J. Vleugels, W.W. Chen, S.G. Huang, J. Eur. Ceram. Soc. 21 (2001) 2903.
[25] N. Hickey, P. Fornasiero, R. Di Monte, J. Kaspar, M. Graziani, G. Dolcetti, Catal. Lett. 72 (2001) 45.
[26] F. Giordano, A. Trovarelli, C. Leitenburg, M. Giona, J. Catal. 193 (2000) 273.
[27] P. Fornasiero, T. Montini, M. Graziani, J. Kaspar, A.B. Hungria, A. Martinez-Arias, J.C. Conesa, Phys. Chem. Chem. Phys. 4 (2002) 149.
[28] N. Hickey, P. Fornasiero, J. Kaspar, J.M. Gatica, S. Bernal, J. Catal. 200 (2001) 181.
[29] H. Vidal, J. Kaspar, M. Pijolat, G. Colon, S. Bernal, A. Cordon, V. Perrichon, F. Fally, Appl. Catal. B 30 (2001) 75.
[30] M. Boaro, C. de Leitenburg, G. Dolcetti, A. Trovarelli, J. Catal. 193 (2000) 338.